J. Fluid Mech. (2003), *vol.* 495, *pp.* 235–253. © 2003 Cambridge University Press
DOI: 10.1017/S0022112003006232 Printed in the United Kingdom

The transverse force on clean and contaminated bubbles rising near a vertical wall at moderate Reynolds number

By FUMIO TAKEMURA[1] AND JACQUES MAGNAUDET[2]

[1]Institute for Energy Utilization, National Institute of Advanced Industrial Science and Technology, 1-2-1 Namiki, Tsukuba, Ibaraki 305-8564, Japan

[2]Institut de Mécanique des Fluides de Toulouse, UMR CNRS/INPT/UPS 5502, 2, Allée Camille Soula, 31400 Toulouse, France

(Received 19 September 2002 and in revised form 18 June 2003)

The transverse migration of both clean and fully contaminated spherical bubbles rising near a plane vertical wall in a quiescent viscous liquid is studied experimentally using an optical technique. Knowing the bubble radius R, rising speed U and separation distance L between the bubble centre and the wall as a function of time, the transverse or lift component of the hydrodynamic force is determined as a function of L/R for Reynolds numbers $Re = 2UR/\nu$ less than 100 (ν is the kinematic viscosity). At low Reynolds number, the lift force is directed away from the wall for both clean and contaminated bubbles and its magnitude is found to be in good agreement with available analytical solutions. For $Re > 1$, contaminated bubbles are still repelled from the wall, but the magnitude of the lift force is always larger than predicted by the low-Re theory, the difference being an increasing function of Re. The behaviour of clean bubbles is markedly different as the experiments reveal that the lift force is directed away from the wall for $Re < 35$ and toward it for higher Re. The differences found in the evolution of the lift force for clean and contaminated bubbles are analysed by considering the relative strength of two hydrodynamical mechanisms of wall interaction, one being due to the vorticity generated at the bubble surface while the other is due to the irrotational dipole associated with the bubble. Empirical correlations based on the strength of these two mechanisms are derived to obtain practical expressions of the lift force as a function of Re and L/R. At high enough Re, clean bubbles rising sufficiently close to the wall are found to bounce very close to it. Based on present and past experimental results, we suggest that this bouncing process is essentially due to the competition between inertial and viscous effects, rather than to bubble deformation as previously believed, and we propose that observations may be explained by considering the effect of the vorticity present in the wall boundary layer. Evaluation of the various contributions involved in the lateral force balance of bouncing bubbles reveals the central role of history effects due to unsteady diffusion of vorticity from the bubble surface.

1. Introduction

When a spherical particle moves parallel to a wall at non-zero Reynolds number, it experiences a transverse or lift force. In the case where the fluid is at rest at infinity, the origin of this force may in general be due to two different mechanisms. At

finite Reynolds number, the vorticity produced at the particle surface diffuses and is transported downstream in the wake. Owing to the presence of the wall, the velocity field induced by this vorticity distribution exhibits some asymmetry with respect to the plane parallel to the wall and containing the particle centre, thus resulting in a transverse force. This mechanism has been studied in detail, both theoretically and experimentally, in the low-but-finite Reynolds-number limit. Cox & Hsu (1977) and Vasseur & Cox (1977) considered the case of rigid spheres, while Takemura *et al.* (2002) (hereinafter referred to as TTMM) explored that of clean bubbles. For both types of particle, the corresponding transverse force is directed away from the wall and is a decreasing function of the separation distance between the particle and the wall. On the other hand, inviscid irrotational theory predicts that the presence of a wall (strictly speaking a symmetry plane) tends to accelerate the flow in the gap separating the sphere from it, thus resulting in a transverse force directed towards the wall (Milne-Thomson 1968, p. 563). A natural question is then which of these two antagonistic effects is controlling the near-wall migration of a particle or a bubble moving parallel to a wall at moderate Reynolds number ($1 < Re < 100$, typically). When a clean spherical bubble rises at large Reynolds number, it is known that the flow about it is almost irrotational, except in a thin boundary layer and a thin wake (Moore 1963). Hence, for high enough Re, we can expect the irrotational mechanism to dominate for such bubbles, so that they should migrate towards the wall. In contrast, the amount of vorticity produced at the surface of a rigid particle is an increasing function of the Reynolds number, so that we expect wake effects to be important for such particles even at moderate-to-large Reynolds number. Thus, the net result of the competition between the two aforementioned effects in this range of Re is *a priori* less clear for rigid particles; nevertheless, compared to the case of clean bubbles, it is likely that the vortical mechanism dominates over a wider range of Reynolds number. Our purpose here is to explore these different situations and the competition between the vortical and the irrotational mechanisms by considering clean and contaminated bubbles.

It is well established that under usual conditions, small bubbles rising in water behave as rigid particles, owing to the adsorption of surfactants at their surface (e.g. Clift, Grace & Weber 1978; Magnaudet & Eames 2000 and references therein). In particular, there is almost no difference between the drag of a contaminated bubble and that of a solid sphere moving at the same Reynolds number. In contrast, the surfaces of bubbles rising in hyperclean water (Duineveld 1995) or in silicone oil (TTMM) remain clean, so that the surrounding liquid is submitted approximately to a shear-free condition at the bubble surface. At low Reynolds number, this difference in the boundary condition does not change the flow structure qualitatively. Consequently, the low-Reynolds-number expression of the lateral force on a clean bubble moving parallel to a wall in a liquid otherwise at rest differs from that on a rigid sphere only by a numerical factor. As shown in TTMM, this factor is $(2/3)^2$, i.e. 0.444 approximately, a prediction confirmed by experiments. The central question we have in mind here concerns the differences in the evolution of the transverse force for the two types of bubble in the inertia-dominated regime, typically $1 < Re < 100$ in the experiments reported below. In this regime, the vorticity generated at the surface of a contaminated bubble increases strongly with Re (at high Re it evolves as $Re^{1/2}$ if the no-slip condition holds), while it increases only weakly with Re in presence of a shear-free condition (the dimensionless vorticity at a shear-free surface of given shape is independent of Re in the limit $Re \to \infty$). Hence, we expect the boundary layer and the wake structure of both types of bubble to become increasingly

different as Re increases, which should result in different evolutions of the near-wall migration.

2. Experimental procedure

The experimental facility, the bubble generation system, the optical technique and the procedure used to measure the evolution of the bubble radius R and rise velocity U parallel to the wall were extensively described in TTMM (see also Takemura & Yabe 1999), so that this description will not be repeated here. The test section is a 500 mm long glass channel with a square cross-section of $50 \times 50\,\mathrm{mm}^2$. The vertical wall (see in TTMM how we ensure verticality) is a stainless steel plate 300 mm long and 40 mm wide inserted in the middle of the cross-section and having its leading edge located 200 mm above the bottom of the test section to avoid disturbances just after bubble generation. The central part of the measurement system is an optical device combining a CCD camera and a microscope and travelling vertically with the rising bubble. The whole optical device is fixed on the vertical displacement system which is driven by a step-by-step motor having enough torque to lift up 10 kg at $150\,\mathrm{mm\,s}^{-1}$. As the total weight of the camera and the microscope is about 2.5 kg, the whole system can move without any vibration. A crucial quantity in the present study is the horizontal distance L separating the bubble from the wall. To locate the wall precisely, we first put the tip of a needle in contact with it, move the needle horizontally along the plate until it comes to the centre of the field of the microscope and focus the microscope on it. This gives us the reference horizontal position (z_0 say) of the micrometric displacement system of the microscope for which the focus coincides with the plate surface. Then, when following a bubble, we merely focus the microscope on it at each vertical location, note the corresponding horizontal position of the focusing system (z_B say) and evaluate the separation distance as $L = z_B - z_0$.

All the experiments are carried out at room temperature and atmospheric pressure using water or silicone oil (dimethyl siloxane polymer; Shinetsu Chemical Co. KF-96) as the carrying liquid. To ensure that bubbles rising in water are contaminated, we introduce $0.1\,\mathrm{mol\,m}^{-3}$ of pentanol ($C_5H_{11}OH$) into the batch of water. Despite this addition, the kinematic viscosity of the solution does not change and is $0.91 \times 10^{-6}\,\mathrm{m}^2\,\mathrm{s}^{-1}$ at 20 °C. We select bubble radii from 50 μm to 450 μm, so that the corresponding bubble Reynolds number ranges approximately from 1 to 100. To analyse the rise of clean bubbles, we use two different silicone oils with kinematic viscosities of 1.08 $10^{-6}\,\mathrm{m}^2\,\mathrm{s}^{-1}$ and 2.65 $10^{-6}\,\mathrm{m}^2\,\mathrm{s}^{-1}$, respectively (hereinafter these two oils are referred to as K1 and K2, respectively). As silicone oils are non-polar liquids, they are not sensitive to the presence of minute amounts of surfactants and they remain naturally 'hydrodynamically clean'. Variations of oil viscosity with temperature are determined and taken into account in the data analysis as explained in TTMM. We select bubble radii from 200 to 400 μm, so that the corresponding Reynolds number ranges approximately from 10 to 90. To obtain an accurate optical description of the bubbles, the resolution of the CCD camera is set to about 6.4 μm per pixel for bubbles with $R > 0.2$ mm. For smaller bubbles, we use a lens with a higher magnification, so that the resolution of the CCD camera is increased up to about 2.5 μm per pixel.

To verify that bubbles rising in silicone oil are clean whereas those rising in water are fully contaminated, we evaluate the drag force acting on bubbles rising far from the wall in both types of liquid. Having determined with the aid of the optical device the bubble radius R and terminal rise velocity far from the wall U_∞, we obtain the experimental Reynolds number $Re_{exp} = 2RU_\infty/\nu$. We can also determine a 'theoretical'

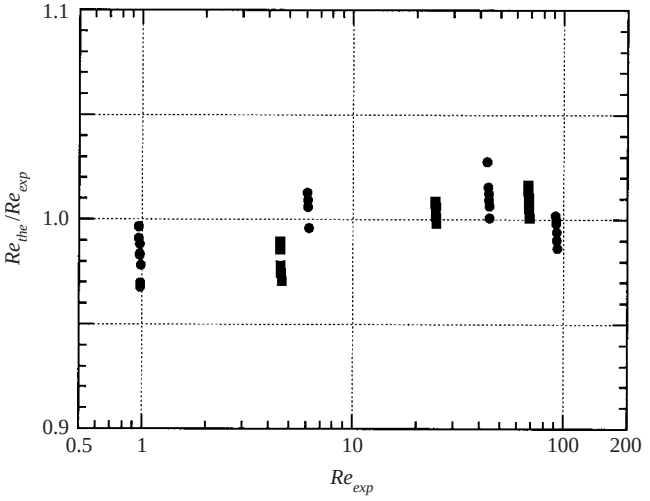

FIGURE 1. Comparison of the theoretical (Re_{the}) and experimental (Re_{exp}) bubble Reynolds number. ●, contaminated water; ■, silicone oil.

Reynolds number Re_{the} by equating a closed-form expression of the drag force F_D to the buoyancy force. For this purpose, we assume that the drag force acting on a contaminated bubble may be expressed using the well-known Schiller–Neumann drag law (Clift *et al.* 1978, p. 111), namely

$$\frac{F_D}{6\pi\mu RU} = f(Re) = 1 + 0.15Re^{0.687}, \tag{1a}$$

where μ is the dynamic viscosity of the liquid. Similarly, we express the drag force on a clean spherical bubble rising at finite Re by using the semi-empirical law proposed by Mei, Klausner & Lawrence (1994), namely

$$\frac{F_D}{4\pi\mu RU} = h(Re) = 1 + \left\{\frac{8}{Re} + \tfrac{1}{2}\left(1 + 3.315Re^{-1/2}\right)\right\}^{-1}. \tag{1b}$$

Equating F_D to the buoyancy force and neglecting the bubble density then yields

$$Re_{the}\,\mathscr{F}(Re_{the}) = \frac{4R^3 g}{9\beta\nu^2}, \tag{2}$$

where $\beta = 1$ and $\mathscr{F} = f$ (resp. $\beta = 2/3$ and $\mathscr{F} = h$) for a contaminated (resp. clean) bubble, and g denotes gravity. Figure 1 shows how the ratio Re_{the}/Re_{exp} obtained by solving (2) evolves with Re_{exp} in both types of liquid. The difference between the experimental and the 'theoretical' Reynolds number never exceeds 3%, which is within the uncertainty on the drag estimate provided by (1*a*, *b*). Hence, bubbles rising in silicone oil can indeed be regarded as clean, whereas those rising in water are fully contaminated and behave like solid spheres.

To evaluate the lift force acting on the bubble, we first calculate the migration speed W by differentiating the time series of the separation distance L with respect to time. In all cases where the transverse force is directed away from the wall, we observed that the migration speed was accurately fitted by an empirical law of the form $W = AL^{-B}$. We determined the coefficients A and B for each series of data and took advantage of this fit to obtain smooth evolutions of W for large separation

distances. To determine the lift coefficient C_L related to the lift force F_L through the definition $F_L = C_L \pi R^2 \rho U^2/2$ (ρ denoting the liquid density), we assume that the vertical (resp. horizontal) drag force exactly balances the buoyancy (resp. lift) force. This quasi-steady approximation was discussed in TTMM and it was shown that transient effects do not play any significant role in the force balance, except very close to the leading edge of the wall. Assuming that this approximation still holds under present conditions, the force balance in the vertical and transverse direction is, respectively,

$$6\beta\pi\mu R\mathscr{F}(Re)U(1 + C_{WU}(L/R, Re)) = \tfrac{4}{3}\pi\rho R^3 g, \tag{3a}$$

$$6\beta\pi\mu R\mathscr{F}(Re)W(1 + C_{WW}(L/R, Re)) = F_L. \tag{3b}$$

Note that in (3*a*,*b*) the exact definition of the Reynolds number is $Re = 2R(U^2 + W^2)^{1/2}/\nu$. However, the inclination angle W/U is always less than 0.02 in our experiments, so that we approximate the bubble Reynolds number as $Re \approx 2RU/\nu$. The first term in the left-hand side of (3*a*,*b*) is the drag force that the bubble would experience if rising at Reynolds number Re along an inclined path in an unbounded domain with the vertical (resp. horizontal) velocity U (resp. W). Terms proportional to $C_{WU}(L/R, Re)$ and $C_{WW}(L/R, Re)$ represent a near-wall correction to the drag force. This correction can be determined analytically only in the limit $Re \to 0$ (see equations (A5) and (A7) of TTMM), or in that of a viscous irrotational flow (Kok 1993). A feature shared by both asymptotic limits is that, to leading-order (i.e. to $O(R/L)$ for $Re \to 0$, and to $O((R/L)^3)$ in the limit considered by Kok), the ratio C_{WW}/C_{WU} is equal to 2; that is the wall-induced correction to the drag of a bubble moving perpendicularly to the wall is twice that on a bubble moving parallel to it.

To obtain a reasonable estimate of C_{WW} at finite Re, we assume that this property holds whatever Re. In the present experiments, the above assumption is unimportant in the case of a contaminated bubble because the effect of the above near-wall correction was found to be significant only for $L/R \leqslant 2.5$, a range of separations which was reached only in presence of a clean bubble (compare the smallest values of L/R in figures 4 and 7 for instance). As the ratio C_{WW}/C_{WU} is known to be equal to 2 for both $Re \to 0$ and $Re \to \infty$ for a clean bubble and no extra mechanism of interaction is expected to occur in between these two limits, the assumption that this ratio does not deviate significantly from 2 at moderate Reynolds number seems sound. Therefore we exploit (3*a*,*b*) as follows. Measurement of R yields the buoyancy force, so that the value of the left-hand side of (3*a*) is known. Having determined experimentally U and W at a given separation L allows us to evaluate Re and $\mathscr{F}(Re)$ using (1*a*) or (1*b*). Then $C_{WU}(Re)$ is straightforwardly obtained using (3*a*) and we evaluate the left-hand side of (3*b*) by assuming $C_{WW}(L/R, Re) = 2C_{WU}(L/R, Re)$.

3. The wall-induced lift force

The photographs of figure 2(*a*) show four typical evolutions of a bubble rising near the vertical wall. The trajectories corresponding to cases (i) to (iii) in figure 2(*a*) are plotted in figure 2(*b*). Series (i) was obtained in silicone oil K2 and the Reynolds number was about 27. The bubble migrates away from the wall with a migration speed decreasing as the separation distance to the wall increases. Similarly, Series (ii) shows that a contaminated bubble rising in water with a Reynolds number of 92 migrates away from the wall. The migration process observed in these two series looks qualitatively similar to the low-Re situation described by Vasseur & Cox (1977) and TTMM. In contrast, in series (iii) taken in silicone oil K1, we observe that

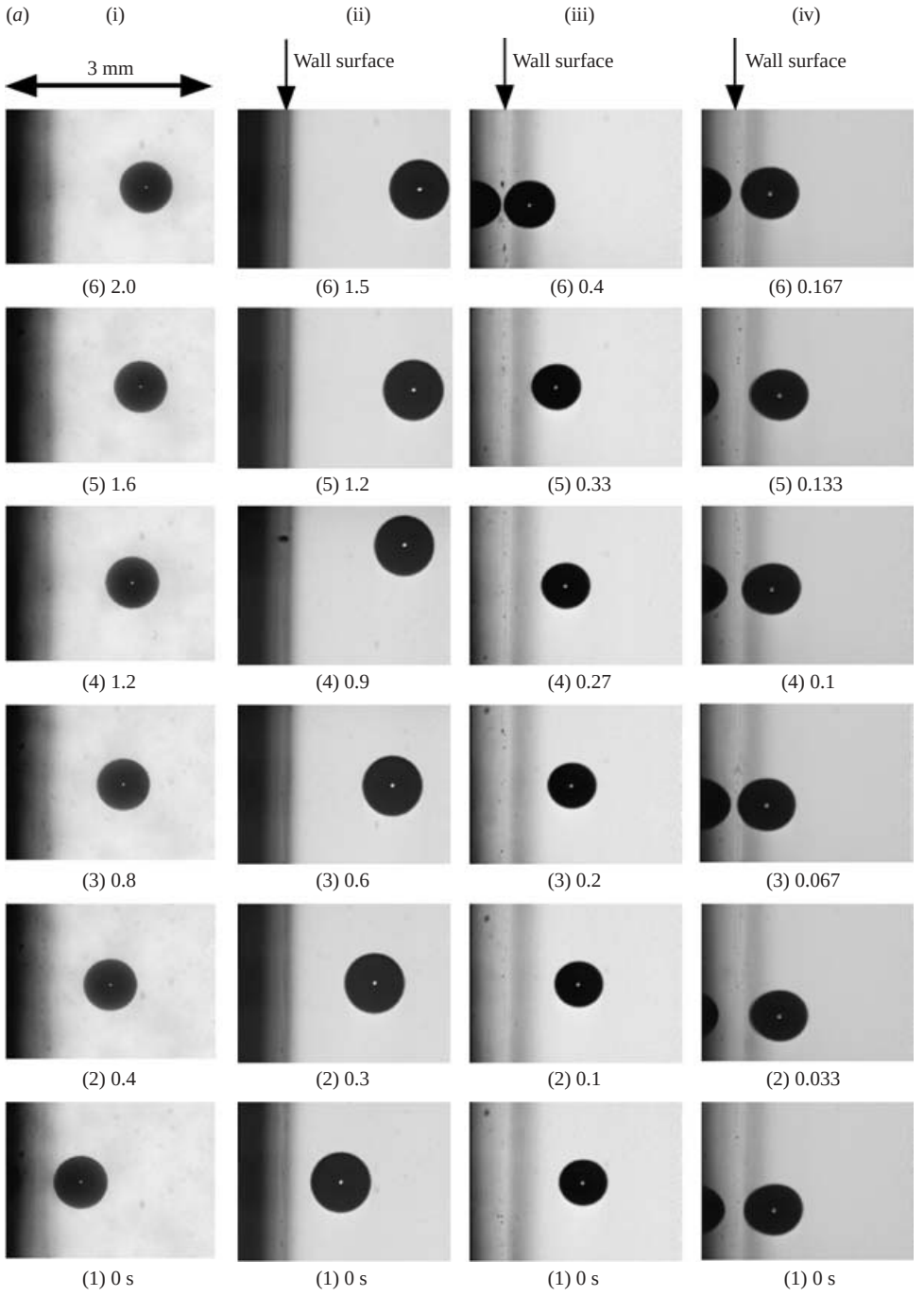

FIGURE 2. (*a*) For caption see facing page.

a clean bubble rising with a Reynolds number of about 85 migrates towards the wall. The evolutions depicted in series (ii) and (iii) for almost identical Reynolds numbers demonstrate that contamination has a dramatic effect on the wall-induced migration at moderate Reynolds number. In case (iii), the trajectory exihits two

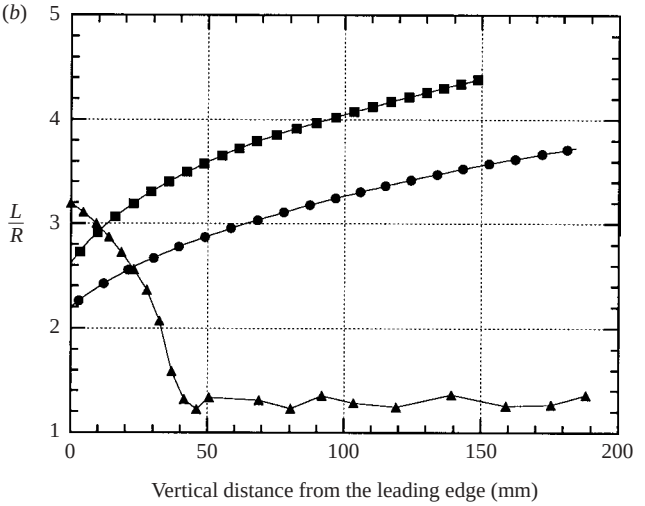

FIGURE 2. (*a*) Series of photographs showing typical bubble evolutions near the wall. (i) silicone oil K2: $R = 0.378$ mm, $U_\infty = 93.3\,\mathrm{mm\,s^{-1}}$, $Re = 26.6$; (ii) water: $R = 0.423$ mm, $U_\infty = 98.7\,\mathrm{mm\,s^{-1}}$, $Re = 92.0$; (iii) silicone oil K1: $R = 0.327$ mm, $U_\infty = 140.0\,\mathrm{mm\,s^{-1}}$, $Re_\infty = 84.8$, $U = 115.0\,\mathrm{mm\,s^{-1}}$, $Re = 70$. (iv) silicone oil K1: $R = 0.385$ mm, $U_\infty = 185.0\,\mathrm{mm\,s^{-1}}$, $Re_\infty = 130.0$. $U = 135.0\,\mathrm{mm\,s^{-1}}$, $Re = 96.25$. (*b*) Trajectories corresponding to cases (i), (ii) and (iii) in (*a*). (i) ●; (ii) ■; (iii) ▲.

markedly different stages. In the first of these, there is a clear attraction towards the wall and the separation distance decreases strongly as the bubble rises along the plate. Then, once the relative separation has reached a value about 1.3, it does not evolve significantly any more and just exhibits small-amplitude oscillations about this equilibrium value. This second stage clearly indicates that the transverse force vanishes for $L/R \approx 1.3$ at the corresponding Reynolds number.

Series (iv) in figure 2(*a*) (also taken in K1) shows a different evolution. Here, the bubble rises very close to the wall and bounces at regular time intervals. Note that the corresponding photographs indicate that the bubble motion is strongly slowed down by the wall since $Re = 96.2$ (based on the local velocity U) and $Re_\infty = 130$ (based on U_∞). Bouncing of a clean bubble rising along a vertical wall has already been reported in the literature, especially by de Vries (2001). We shall comment on this situation in more detail in § 4.

3.1. *Contaminated bubble*

Figure 3 shows the evolution of the lift coefficient C_L *vs.* the dimensionless separation $L^* = LU/\nu$ for Reynolds numbers ranging from 1 to 100, approximately (see TTMM for details concerning the determination of error bars). The quantity L^* compares the distance between the bubble and the wall to the viscous length ν/U and is appropriate for $Re < 1$ because values of L^* larger (resp. smaller) than unity then indicate that the wall lies in the Oseen (resp. Stokes) region of the flow disturbance due to the bubble, i.e. inertial (resp. viscous) effects dominate near the wall. In the regime ($Re \ll 1$, $L^* \gg 1$), Vasseur & Cox (1977) (for $\beta = 1$) and TTMM (for $\beta = 2/3$) showed that the lift coefficient is a function of L^* only, i.e. $C_L = C_{L0}(L^*)$ with

$$C_{L0}(L^*) = \frac{9\beta^2}{\pi L^{*2}} \int_0^\infty \int_0^{2\pi} \frac{\chi + \lambda}{\chi - \lambda} (\mathrm{e}^{-\lambda} - \mathrm{e}^{-\chi})^2 \lambda \, \mathrm{d}\lambda \, \mathrm{d}\phi, \tag{4}$$

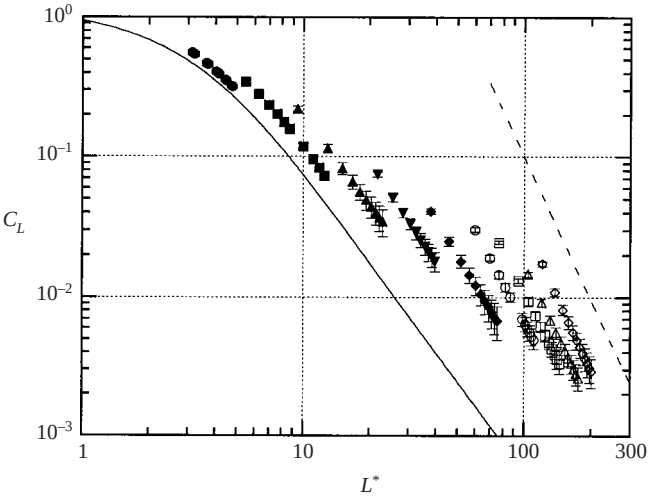

FIGURE 3. The wall-induced lift coefficient C_L of a contaminated bubble. ●, $Re_\infty = 0.96$; ■, $Re_\infty = 2.5$; ▲, $Re_\infty = 6.1$; ▼, $Re_\infty = 14.3$; ◆, $Re_\infty = 24.9$; ○, $Re_\infty = 43.8$; □, $Re_\infty = 57.5$; △, $Re_\infty = 72.9$; ◇, $Re_\infty = 92.0$; ——, numerical integration of (4) ($\beta = 1$); - - -, $C_L \propto L^{*-3.4}$.

where $\chi^2 = \lambda^2 + \mathrm{i}\lambda L^* \cos\phi$ with $\mathrm{i}^2 = -1$. Here, we still use the dimensionless separation L^* in order to see how C_L compares with C_{L0} at moderate Reynolds number. Note that, owing to the limited lateral excursion of our optical device (20 mm), our data cover only a limited range of L^* (i.e. of L/R) for each value of Re. As shown in figure 3, values of C_L corresponding to $Re = 0.96$ are in good agreement with the expression of Vasseur & Cox (1977), thus providing additional confirmation that bubbles are fully contaminated. For larger Re, the magnitude of the lift coefficient strongly decreases and is about two orders of magnitude smaller for $Re = O(10^2)$ than for $Re = O(1)$. Nevertheless, this decrease is much less severe than predicted by the low-Re solution and figure 3 indicates that the ratio C_L/C_{L0} reaches values about 40 for $Re = 92$. Hence, it is clear that for Reynolds numbers larger than unity, C_L is a function of both L^* and Re. To interpret the variations of C_L with Re and correlate approximately its values to L^* and Re, we note that figure 3 suggests that, to a first approximation, the low-Re solution captures reasonably well the dependency of C_L with respect to L^* for a given Re in the range $1 \leqslant Re \leqslant 100$. A more careful examination shows that for $L^* > 10$, the slope of the experimental 'curves' decreases with Re, ranging from about -2.1 for $Re < 10$ (this is the slope of the continous line in the corresponding range of L^*) to about -3.4 for $Re = O(10^2)$ (corresponding to the slope of the dashed line). We shall come back to this feature later, but shall ignore it for now. Hence, we first seek to approximate C_L by writing

$$C_L = C_{L0}(L^*)\mathscr{G}(Re). \tag{5}$$

To interpret physically the function $\mathscr{G}(Re)$, it is again useful to come back to the low-Re situation. At low Reynolds number, the main difference between a clean bubble and a rigid sphere lies in the intensity of the associated Stokeslet. More precisely, the strength of the Stokeslet of a clean bubble is 2/3 that of a rigid sphere, a direct consequence of this being that the maximum vorticity at the surface of a clean bubble is 2/3 that on a rigid sphere. This is also why the drag force is proportional to the factor β, as implied by (1a, b). In the same regime, (4) shows that the migration force

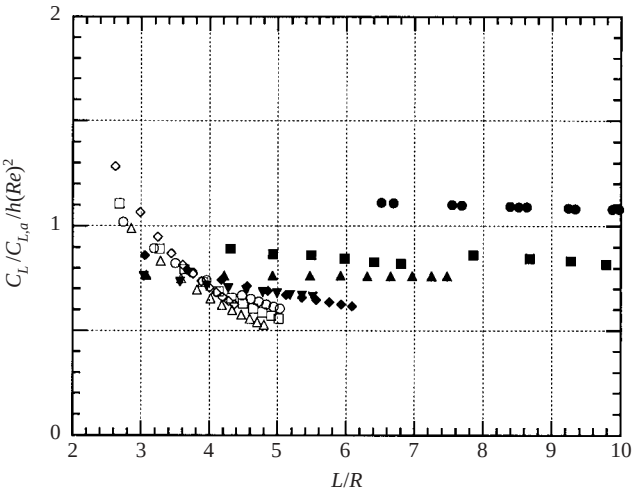

FIGURE 4. The wall-induced lift coefficient C_L of a contaminated bubble normalized by $C_{L0}(L^*)a^2(Re)$. For caption see figure 3.

is proportional to β^2. As explained in TTMM (see also Legendre & Magnaudet 1997), this is because the lift force is due to the interaction of the wall with the far-field disturbance induced by the Stokeslet. The strength of this far-field disturbance is obviously proportional to that of the Stokeslet, i.e. β. Moreover, a unit velocity in the far field results in a hydrodynamic force proportional to β. Combining both steps of this reasoning shows immediately that the resulting lift force is necessarily proportional to β^2. Note that a slightly more elaborated physical reasoning also allows us to understand the asymptotic variation of C_L with L^* for $L^* \gg 1$ in the low-Re regime. Given the $x^{1/2}$ growth of the wake with the downstream distance x to the particle and the self-similar evolution of the velocity disturbance on the wake axis $\Delta u \propto F_D/(4\pi\mu x)$ in the far wake (Batchelor 1967, pp. 243, 349), it is straightforward to show that the velocity defect in the wake reaches the wall for $x \sim ReL^2/R$, so that $\Delta u(ReL^2/R) \propto (R/L)^2 F_D/(4\pi\mu RRe)$ in this region. Assuming that the lift force is directly proportional to this value of Δu, i.e. $F_L \sim \beta\mu R\Delta u(ReL^2/R)$, and noting that $F_D \sim \beta\mu RU$, we find immediately $C_{L0} \sim \beta^2 L^{*-2}$, which is indeed the asymptotic behaviour of (4) for $L^* \gg 1$, as shown mathematically by Vasseur & Cox (1977).

We now assume that at moderate Re the transverse force on a rigid sphere or a contaminated bubble is still essentially due to the disturbance produced by the interaction of the wall with the far-field velocity resulting from the vorticity generated at the particle surface. As the far wake of a non-lifting body has a structure similar to that of the Oseen wake (Batchelor 1967, pp. 351–352), we expect that the most noticeable change compared to the low-Re situation lies in the strength of the vorticity produced on the particle. Hence, following the above line of reasoning, we should have $\mathscr{G}(Re) = a^2(Re)$ in (5), with $a(Re)$ characterizing the strength of the vorticity at the bubble surface normalized by its value in the creeping flow limit. A typical and simple measure of this strength may be obtained by defining $a(Re)$ as the ratio $\omega_{max}(Re)/\omega_{max}(Re = 0)$, where ω_{max} is the maximum vorticity at the surface of the bubble. The function $a(Re)$ can then be approximated easily by examining values of ω_{max} found in available numerical simulations of the uniform unbounded flow past a rigid sphere. Using, for instance, data from Magnaudet, Rivero & Fabre (1995), we find $a(Re) \approx 1 + 0.6Re^{1/2} - 0.55Re^{0.08}$. Figure 4 shows how $C_L(Re)/C_{L0}(L^*)a^2(Re)$

evolves with Re and L/R. This ratio does not deviate from unity by more than 50% over the whole range of Re covered by our experiments, thus reinforcing our physical interpretation of the wall-induced migration mechanism.

Not surprisingly, the maximum deviations from unity in figure 4 are encountered for the largest values of Re and L/R, and they suggest that our crude model overestimates the tiny lift force that subsists in this regime. The reason for these deviations may be understood by coming back to the physical argument developed above. While the expression of the velocity defect Δu in the wake is still valid, it is likely that at high enough Reynolds number, the lift force is proportional to Δu^2 rather than to Δu as assumed in the above low-Re reasoning. If so, it immediately turns out that for a given Re, $C_L(Re \to \infty)$ is proportional to $(L/R)^{-4}$ rather than to $(L/R)^{-2}$. A similar conclusion may be obtained by considering the nature of the disturbance flow near the bubble and analysing how this disturbance interacts with the wall, and at which order (in terms of R/L) it produces an asymmetry of the vorticity distribution with respect to the plane parallel to the wall and containing the bubble centre. At low Re, the disturbance flow is merely that produced by a Stokeslet, and it is well known that the interaction of a Stokeslet with a wall induces an asymmetric flow about the bubble (in the form of a linear straining flow and a stresslet) at $O((L/R)^{-2})$ (e.g. Magnaudet, Takagi & Legendre 2003). In contrast, at high Re, the flow outside the boundary layer and the wake is irrotational, so that the disturbance is essentially that produced by a dipole. Because of its faster decay as the distance to the bubble centre increases, the interaction of such a disturbance with the wall produces a linear straining flow (and a quadrupole) only at $O((L/R)^{-4})$. Hence at high Re, the boundary layer around the bubble (and therefore the wake) exhibits an asymmetry only at $O((L/R)^{-4})$, so that the transverse force associated with the vortical mechanism considered up to now decays much faster with increasing L/R than in the low-Re regime. What the present experimental results suggest is that for $Re = O(10^2)$ the situation is intermediate between the above two asymptotic limits, since figure 3 shows that for $Re = O(10^2)$ the transverse force decays approximately as $F_L \sim (L/R)^{-3.4}$ (see the slope of the dashed line). To take into account the above transition between the low- and high-Re regimes, we may simply multiply expression (5) by a factor $(L/\gamma R)^{g(Re)}$ where γ is an empirical constant and $g(Re)$ is an empirical function giving the correct asymptotic behaviour of the transverse force at both low and high Reynolds number, i.e. $g(0) = 0$ and $g(Re \to \infty) = -2$ (since $C_{L0}(L^*) \propto (L/R)^{-2}$ for $L^* \to \infty$). According to present experimental results, we have $g(Re) \approx -2.0 \tanh(0.01Re)$ and $\gamma \approx 3.0$. Summarizing, the complete model of the lift coefficient becomes

$$C_L = C_{L0}(L^*)a^2(Re)(L/\gamma R)^{g(Re)}, \tag{6a}$$

with

$$\gamma \approx 3.0, \quad g(Re) \approx -2.0 \tanh(0.01Re), \quad a(Re) \approx 1 + 0.6Re^{1/2} - 0.55Re^{0.08}. \tag{6b}$$

Moreover, for practical purposes it is worth noting that the exact expression (4) for $C_{L0}(L^*)$ is accurately fitted by

$$C_{L0}(L^*) = \begin{cases} (9/8 + 5.78\,10^{-6}L^{*4.58})\beta^2 \exp(-0.292L^*) & \text{for } 0 < L^* < 10, \\ 8.94\beta^2 L^{*-2.09} & \text{for } 10 \leqslant L^* < 300. \end{cases} \tag{6c}$$

Figure 5 shows how this improved model compares with the experimental results. The prediction (6a–c) is almost independent of L/R and does not deviate from experimental values by more than approximately 20%, which is the typical order of

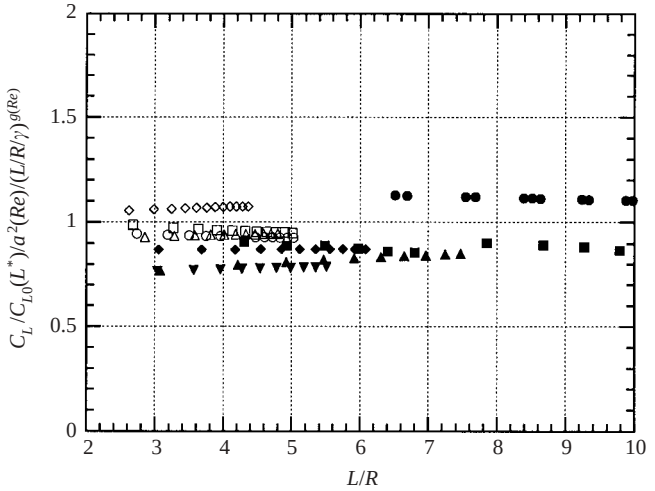

FIGURE 5. The wall-induced lift coefficient C_L of a contaminated bubble normalized by $C_{L0}(L^*)a^2(Re)(L/\gamma R)^{g(Re)}$. For caption see figure 3.

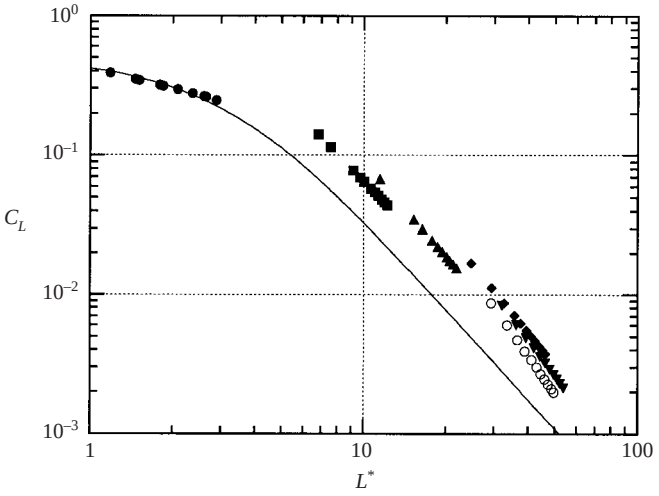

FIGURE 6. The wall-induced lift coefficient of a clean bubble for $Re < 30.0$. ●, $Re_\infty = 0.8$; ■, $Re_\infty = 4.6$; ▲, $Re_\infty = 7.2$; ◆, $Re_\infty = 16.0$; ▼, $Re_\infty = 24.9$; ○, $Re_\infty = 26.6$; ——, numerical integration of (4) ($\beta = 2/3$).

magnitude of the experimental uncertainty on C_L. The fit could probably be improved by optimizing γ, $a(Re)$ and $g(Re)$ using experimental and numerical data. However, our present purpose is mainly to present simple physical arguments by which a reasonable scaling of the lift force can be obtained. Keeping in mind this objective and the significant uncertainty on our measurements, we shall not try to perform such an optimization here.

3.2. *Clean bubble*

Figure 6 displays the lift coefficient of a clean bubble as a function of L^* and Re for $Re < 30$ (the three sets of data corresponding to $Re < 10$ were taken from TTMM). The migration force is still directed away from the wall. Its intensity agrees with

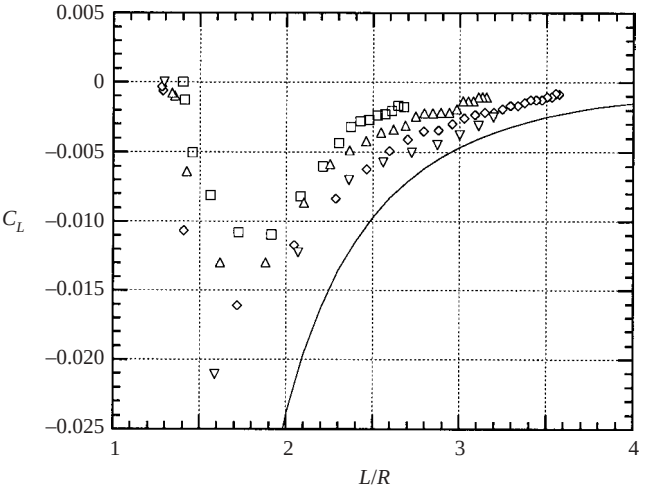

FIGURE 7. The wall-induced lift coefficient of a clean bubble for $45 < Re < 90$. □, $Re_\infty = 48.6$; △, $Re_\infty = 58.0$; ◇, $Re_\infty = 68.9$; ▽, $Re_\infty = 84.8$; ——, equation (7).

the low-Re expression (4) (with $\beta = 2/3$) up to $Re = O(1)$ and becomes larger than predicted by (4) for larger Reynolds numbers. Nevertheless, in contrast with the evolution observed for a contaminated bubble, the ratio $C_L(Re)/C_{L0}(L^*)$ does not exceed a value of 3.0; moreover, this ratio tends to decrease for the highest values of Re because of the transition from a -2 slope to a -4 slope, as discussed above.

Figure 7 shows the variations of C_L *vs.* L/R at somewhat higher Reynolds number, namely $40 < Re < 90$. The corresponding 'curves' are totally different from those discussed up to now. The lift coefficient is negative in the whole range of L/R over which we were able to determine the transverse velocity, indicating that the interaction force is now directed towards the wall. For a given L/R, the absolute value of C_L increases with Re and saturates for the highest Reynolds numbers reached in the experiment. For a given Re, $|C_L|$ decreases rapidly as the separation increases and is less than 10^{-3} for $L/R > 4$. We also note that the lift coefficient exhibits a minimum near $L/R = 1.6$. For smaller separations, the few experimental points that were obtained indicate that $|C_L|$ decreases sharply as the wall is approached. A stable equilibrium position exists near $L/R = 1.3$, in line with the trajectory (iii) displayed in figure 2(*b*). As we could not inject bubbles extremely close to the wall, the vanishing of the lift force for $L/R \approx 1.3$ prevents non-bouncing bubbles to enter the region $L/R < 1.3$; this is why no data point is found in this region in figure 7.

The physical mechanism that gives rise to a negative, i.e. attractive, lift force is undoubtedly related to the well-known feature that, according to irrotational flow theory, two spheres rising side-by-side (or equivalently a sphere in presence of a symmetry plane) are attracted along their line of centres because the fluid velocity reaches a maximum between them, thus inducing a pressure gradient directed away from the symmetry plane. Once the corresponding velocity potential is known, the irrotational interaction or lift coefficient $C_{L\infty}$ may be evaluated, yielding (Miloh 1977; Biesheuvel & van Wijngaarden 1982; Kok 1993)

$$C_{L\infty} = -\frac{3}{8}\left(\frac{R}{L}\right)^4\left\{1 + \frac{1}{8}\left(\frac{R}{L}\right)^3 + \frac{1}{6}\left(\frac{R}{L}\right)^5\right\} + O\left(\frac{R}{L}\right)^{10}. \qquad (7)$$

What figures 6 and 7 suggest is that the vortical mechanism described in § 3.1 dominates the interaction process for $Re < 30$ while the irrotational mechanism becomes dominant at higher Re, except very close to the wall. This is in line with the fact that as Re increases to infinity, the strength of the vorticity produced at the surface of a clean spherical bubble remains bounded (see below), and that the flow field past the bubble becomes close to that predicted by irrotational theory, except in a thin boundary layer and a thin wake (Moore 1963).

To analyse the variations of C_L over the whole range of Re corresponding to figures 6 and 7, we assume that for moderate separations the total lift force mainly results from the linear superposition of the vortical and irrotational mechanisms described above. Following the procedure used in § 3.1, we estimate the strength of the vortical mechanism through (6*a–c*) (with $\beta = 2/3$) now with $a(Re)$ replaced by $b(Re)$, the function $b(Re)$ representing the relative strength $\omega_{max}(Re)/\omega_{max}(Re = 0)$ of the maximum vorticity at the buble surface. Using again numerical data from Magnaudet *et al.* (1995) for shear-free bubbles, we find $b(Re) \approx 1 + 2.0 \tanh(0.17Re^{0.4} - 0.12Re^{0.05})$ (following Batchelor 1967, p. 366, the vorticity on a spherical shear-free surface is $3U/R$ for $Re \to \infty$, so that $b(Re \to \infty) = 3$). To estimate the strength of the irrotational mechanism, we may use results from direct numerical simulations for the local pressure coefficient $C_P = 2(P - P_\infty)/\rho U^2$ at the bubble surface. More precisely, selecting an angular position θ on the bubble and examining how $C_P(\theta)$ varies with Re when the bubble rises in an unbounded domain yields a direct information on the strength of the dipole associated with the irrotational contribution to the flow about it. For instance C_P is zero on the equatorial plane of the bubble ($\theta = \pi/2$) under creeping flow conditions (i.e. when the strength of the dipole is zero) and becomes equal to $-5/4$ in the limit of irrotational flow. According to the numerical results of Magnaudet *et al.* (1995), we find that $-4C_P(\pi/2)/5$ evolves approximately as $c(Re) = 1 - \exp(-0.22Re^{0.45})$. Note that applying the same procedure to the case of a contaminated bubble suggests that the relative strength of the dipole ranges from zero at low Re to 0.4 at high Re; hence, in this case, the irrotational mechanism yields only a small correction to the vortical effect described in § 3.1 over the whole range of L/R and Re covered by our experiments. In contrast, this contribution becomes certainly crucially important at higher Re because (6*a*, *b*) and (4) suggest that the vortical effect is proportional to $Re^{-1}(L/R)^{-4}$ for $Re \to \infty$, whereas the attractive irrotational effect is merely proportional to $(L/R)^{-4}$ and eventually dominates when the Reynolds number is large enough. This is in line with the numerical results of Kim, Elgobashi & Sirignano (1993) who performed direct numerical simulations of the side-by-side motion of two rigid spheres, and observed that the interaction force is attractive for large enough Re and L/R.

Collecting the above ingredients, our model for the lift coefficient on a clean spherical bubble rising at moderate Re becomes

$$C_{LM}\left(Re, \frac{R}{L}\right) = b^2(Re)C_{L0}(L^*)(L/\gamma R)^{g(Re)} + c(Re)C_{L\infty}\left(\frac{R}{L}\right) \tag{8}$$

Figure 8 shows how C_{LM} compares with the measured lift coefficient for all data points reported in figures 6 and 7. It turns out that in spite of a significant dispersion for $2.5 < L/R < 3.5$ due to the scattering among the small negative values of C_L in this range of separation (see figure 7), the ratio C_L/C_{LM} is about 1 as we expected from the previous analysis, except for small separations, typically $L/R < 1.8$. This confirms that in most cases the wall-induced lateral motion of a clean spherical bubble rising

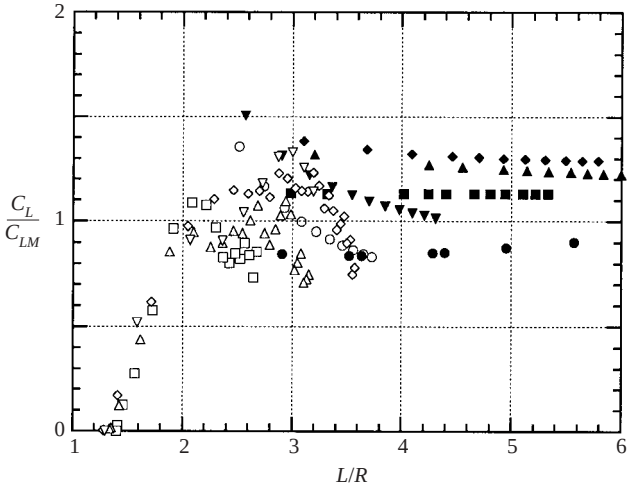

FIGURE 8. The wall-induced lift coefficient C_L of a clean bubble normalized by C_{LM}. For legend see figures 6 and 7.

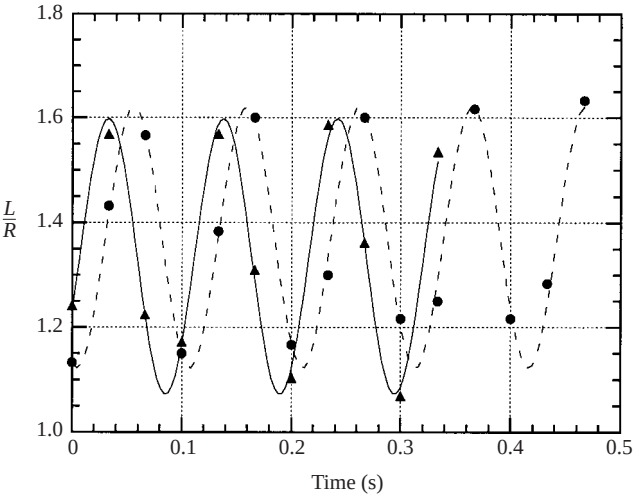

FIGURE 9. Two typical trajectories corresponding to case (iv) in figure 2(*a*). ●, ▲, experimental data; ——, $L(t)/R = 1.34 + 0.263\sin(60.1t)$; - - -, $L(t)/R = 1.27 + 0.250\sin(61.1t)$.

at moderate Re may be understood as resulting mostly from a linear superposition of the attractive irrotational mechanism and the repulsive vortical effect.

4. Bouncing of clean bubbles

We saw in figure 2(*a*) that clean bubbles with a high enough Reynolds number may bounce on the wall or very close to it. Figure 9, in which two of the corresponding trajectories are reported, allows us to specify some features of the bouncing phenomenon. First, the excellent agreement obtained by approaching the observed trajectories with a sinusoidal fit indicates that the motion is periodic with a frequency about 9.65 Hz. Secondly, as the minima of L/R are about 1.12 and 1.07, respectively, we have a clear indication that the bubbles do not touch the wall. Hence, the

bouncing observed in our experiments is purely hydrodynamical. As suggested by the photographs of series (iv) in figure 2(*a*), the bouncing bubbles are slightly deformed, the maximum deformation obtained from the ratio of the major and minor axes being about 8% in this series (see TTMM for details about the determination of the deformation). It is then tempting to attribute the occurrence of the bouncing phenomenon to this deformation. Based on previous work devoted to bouncing and coalesence of a pair of bubbles moving along their line of centres (e.g. Tsao & Koch 1994), de Vries (2001) concluded that in pure water, bubbles bounce or slide along a vertical wall depending on whether the value of the Weber number based on the horizontal velocity W is larger or smaller than a critical value. Moreover, the deformation-induced migration of a bubble rising near a vertical wall was evaluated in the limit $Re \to 0$ by Magnaudet *et al.* (2003), and they showed that it does provide a repulsive contribution to the overall lift force.

Nevertheless, reconsidering de Vries' observations in water together with results reported here in silicone oil K1 suggests a different interpretation. The comparison is particularly revealing for these two fluids because they have roughly the same physical properties, except for surface tension which is about 4.3 times smaller in K1. In de Vries' experiments, the smallest bouncing bubble had a radius of 0.40 mm, a near-wall Reynolds number $Re \approx 90$, and a Weber number $We = 2\,\rho\, U^2 R/\sigma \approx 0.14$, σ being the surface tension. Here, we may say thet the onset of bouncing occurs for the bubble shown in series (iii) of figure 2(*a*), as we could not discern any near-wall oscillation on the trajectory of a slightly smaller bubble with $Re = 65$. In series (iii), the bubble has a radius of 0.327 mm, a Reynolds number about 70, and a Weber number about 0.41. Therefore, comparing with de Vries's results we see that the critical Reynolds number is in the same range in both fluids, whereas the critical Weber number is about three times larger in K1 than in pure water. This strongly suggests that the critical condition for the occurrence of bouncing has more to do with the ratio of inertial to viscous effects than with that of inertial to capillary effects.

Based on this remark, our interpretation is that the essential near-wall repulsive effect that induces the bouncing of nearly spherical clean bubbles when they rise parallel to a wall is due to the shear rate existing in the gap between the bubble and the wall. The thickness of the wall boundary layer is typically $0.1R$ for $Re = O(10^2)$. Owing to the structure of the irrotational flow past a sphere, the vertical velocity is about $-U/2$ on the equator of the bubble (the velocity is directed downwards in this plane). Hence, when $L/R \to 1$, the vertical velocity in the equatorial plane of the bubble has to decrease from zero at the wall to $O(-U/2)$ at the edge of the boundary layer, yielding a wall vorticity about $-5U/R$. There is also a second boundary layer of similar thickness on the bubble, the existence of which is required to satisfy the shear-free boundary condition at the bubble surface (Moore 1963). The corresponding vorticity is about $3U/R$ as we saw above, and it reduces the negative vertical velocity by $O(Re^{-1/2}U)$ at the bubble surface. When $L/R \to 1$, the two boundary layers interact and the flow in the gap looks roughly like a lubrication flow of Reynolds number

$$Re_l \approx \frac{U}{2}\frac{(L-R)}{\nu} = \frac{Re}{4}\left(\frac{L}{R} - 1\right).$$

This estimate yields $Re_l \approx 2.5$ for $Re = 10^2$ and $L/R = 1.1$, showing that viscous effects play a large role in the gap. Compared to the irrotational prediction, it is clear that the two boundary layers reduce the maximum velocity in the gap. Since the existence of an absolute maximum of the vertical velocity in the gap is the source of the

attractive interaction force in the irrotational limit, we infer that as L/R decreases, these boundary layers (especially that due to the no-slip condition at the wall) reduce the attractive force and finally change its sign for small enough separations. More experiments are clearly required to settle the matter definitely and the effectiveness of the mechanism just described has to be studied specifically, but we believe that the arguments presented here strongly support this scenario based on the competition between viscous and inertial effects.

Obviously the above 'boundary layer' effect also exists for contaminated bubbles and rigid spheres and is even stronger for them than for clean bubbles because the vorticity at the particle surface is much larger. Nevertheless, we saw that in presence of a no-slip condition at the bubble surface, the vortical repulsive effect dominates over the irrotational attractive mechanism at moderate Reynolds number; hence, compared to the case of clean bubbles, the bouncing phenomenon can only occur at much higher Re for rigid particles. Under such conditions, the picture is probably much more complicated than that described here because the wake is turbulent, so that mechanisms not considered here are involved in the wall–particle interaction process.

Finally, it is of interest to discuss the transverse force balance on the bouncing bubbles corresponding to figure 9. As we saw, the evolution of the distance $L(t)$ separating them from the wall is accurately fitted in the form $L(t)/R = \varepsilon_0 + \varepsilon \sin \omega t$ with $\varepsilon_0 \approx 1.30 \pm 0.03$, $\varepsilon \approx 0.256 \pm 0.005$, $\omega \approx 60.6 \pm 0.5$ Hz. Then it turns out that the dimensionless radian frequency $\omega R^2/\nu$ is about 8.3, which implies that effects of temporal acceleration are about one order of magnitude larger than viscous effects and cannot be neglected in the force balance. In other words, the quasi-steady approximation (3b) that we used up to now to evaluate the lift force does not hold when bubbles bounce. The correct force balance must include the added-mass force resulting from the lateral acceleration of the liquid displaced by the bubble, as well as the so-called history contribution to the lateral drag force due to the unsteady diffusion of the vorticity about the bubble. We then write

$$\tfrac{4}{3}\pi R^3 \rho C_M \frac{\mathrm{d}W}{\mathrm{d}t} + 4\pi\mu R \left[h(Re) W (1 + C_{WW}) + \int_{-\infty}^{t} K(t-\tau) \frac{\mathrm{d}W}{\mathrm{d}\tau}\, \mathrm{d}\tau \right] = \pi R^2 \rho C_L \frac{U^2}{2}. \quad (9)$$

In (9), $K(t-\tau)$ is the kernel of the history contribution, $h(Re)$ is the finite-Re correction to the quasi-steady drag force as given by (1b), C_M is the added-mass coefficient corresponding to a sphere moving perpendicularly to a plane ($C_M \approx (1+3(R/L)^3/8)/2$, Milne-Thomson 1968, p. 563), and C_{WW} is the corresponding near-wall correction to the quasi-steady drag force on a high-Re spherical bubble ($C_{WW} \approx 3(R/L)^3/4$, Kok 1993). The history kernel is only known analytically in the time domain in the limit of an unbounded unsteady Stokes flow (Yang & Leal 1991), in which case $K(t-\tau) = 2\mathrm{erfc}[3(\nu(t-\tau)/R^2)^{1/2}] \exp(9\nu(t-\tau)/R^2)$. Mei & Klausner (1992) and Lovalenti & Brady (1993) studied in detail the long-time effect of inertial corrections on this kernel. Based on their results, Mei *et al.* (1994) proposed an empirical form of $K(t-\tau)$ supposed to be valid whatever the time lag $t-\tau$ and the bubble Reynolds number Re.

Rather than attempting to check these various forms of the history kernel, we may find some insight into the magnitude and influence of the history force by evaluating all other contributions in (9). For this purpose, using the above expression for $L(t)$, we deduce $W = \varepsilon R \omega \cos \omega t$, $\mathrm{d}W/\mathrm{d}t = -\varepsilon R \omega^2 \sin \omega t$. Moreover, figure 7 suggests that it is reasonable to consider that the quasi-steady lift coefficient evolves linearly in

the range $1.3 \leqslant L/R \leqslant 1.6$. Assuming that this is still the case for smaller separations, we have approximately $C_L \approx -0.07(L/R - \varepsilon_0)$ for L/R in the range $\varepsilon_0 \pm \varepsilon$. Note that if we neglect the possible changes of the rise velocity U with L/R within this range, this linear variation of C_L is compatible with the existence of a sinusoidal evolution of the separation distance $L(t)$. We are now in a position to evaluate the order of magnitude of the various contributions in (9). To make the comparison with C_L easy, we normalize each of them by $\pi R^2 \rho U^2/2$. When $L/R = \varepsilon_0$, the lift force and the added-mass force both vanish. The force balance (9) implies that the history contribution then exactly balances the quasi-steady drag whose magnitude is $\pm 16h(Re)(1 + C_{WW})\varepsilon R\omega/URe \approx \pm 0.023$. When the separation reaches its maximum, i.e. $L/R = \varepsilon_0 + \varepsilon$, the lateral component of the quasi-steady drag is zero, the lift coefficient is about -0.018 and the dimensionless added-mass force is $-(8/3)\varepsilon C_M(R\omega/U)^2 \approx -0.011$. Hence, the dimensionless history force must be about -0.007. Similarly, for $L/R = \varepsilon_0 - \varepsilon$, the history contribution should be about 0.005, the added-mass force then being somewhat stronger than for $L/R = \varepsilon_0 + \varepsilon$, owing to the increase of C_M with decreasing separations. Averaging the last two results yields approximately

$$\frac{1}{U}\int_{-\infty}^{t} K(t-\tau)\frac{\mathrm{d}W}{\mathrm{d}\tau}\,\mathrm{d}\tau \approx -0.14\cos\omega t - 0.035\sin\omega t.$$

Compared with the relative value of all other three lateral forces, we see that the history contribution has a similar or even larger magnitude. The physical origin of such a significant lateral component of the history force may be understood by noting that the large value of $\omega R^2/\nu$ implies that the frequency of the lateral motion is too high for the bubble wake to be perfectly aligned at all times with the bubble velocity. That is, there is some time-dependent misalignment between the wake and the instantaneous angle $W(t)/U$ of the bubble path, which necessarily results in a lateral force. To conclude, the above analysis shows that the lateral history force can by no means be neglected in the force balance (9), especially for $L/R \approx \varepsilon_0$. In other words, any Lagrangian computation of the bubble motion in which the history contribution would be either neglected or inaccurately modelled would fail to reproduce correctly the trajectories displayed in figure 9.

5. Conclusions

We have studied experimentally the wall-induced migration of bubbles rising near a vertical wall in a quiescent liquid in the regime $1 \leqslant Re \leqslant 100$. Using silicone oil and water artificially contaminated by pentanol allowed us to produce both clean and fully contaminated bubbles. Within the range covered by our experimental conditions, the latter are always repelled by the wall and the corresponding repulsive force decreases with increasing Re and L/R. We showed that, provided a correction factor is introduced to take into account the variation of the amount of vorticity produced at the bubble surface with Re, the corresponding transverse force scales fairly well with the low-Re expression derived by Vasseur & Cox (1977). This agreement led us to conclude that for moderate Re, the repulsive wall-induced force acting on rigid spheres and contaminated spherical bubbles is still due to the interaction of the wall with the far-field of the particle wake. We also showed that since the near-field disturbance produced by the bubble changes from that associated to a Stokeslet at low Re to that produced by a dipole at high Re, the dependency of the transverse force with respect to the relative separation L/R must change from $(L/R)^{-2}$ to $(L/R)^{-4}$ as

Re increases. Based on this argument, we introduced an empirical correction into our initial model and obtained an improved agreement with experiments.

The case of clean bubbles was found to be more complex, since bubbles corresponding approximately to $Re < 35$ were found to be repelled by the wall whereas those corresponding to larger Reynolds number are attracted for most values of L/R. We guessed that the repulsion had the same origin as that observed for contaminated bubbles, whereas we attributed the attractive force to the lateral pressure gradient predicted by irrotational flow theory. To check this idea we built a crude model combining linearly both mechanisms, and we estimated the strength of both of them through empirical functions of *Re* extracted from available numerical simulations. This model was found to reproduce correctly the experimental tendencies for moderate separations ($L/R > 1.8$) over the whole range of *Re*. For large enough *Re* and small separations, typically $Re > 85$ and $L/R < 1.6$, experiments showed that bubbles slightly deform and bounce very close to the wall. Previous studies analysed the bouncing mechanism as resulting from this deformation; however, a comparison of present data with de Vries' (2001) results obtained in pure water suggests that the critical condition for bouncing is related to the rise Reynolds number rather than to the Weber number. Based on this finding and on a crude analysis of the flow structure in the gap between the bubble and the wall, we guess that a boundary-layer effect that reduces the maximum vertical velocity in the gap is responsible for the bouncing mechanism, without any need to invoke deformation. We also used the detailed data obtained with bouncing bubbles to analyse the magnitude of the various contributions in the transverse force balance. This analysis revealed that the history force plays a crucial role, especially near the location where the lift force vanishes, and must accurately be modelled in order for the periodic lateral motion associated with the trajectories of bouncing bubbles to be properly predicted.

Present results clarify some of the physical mechanisms that contribute to the wall-induced migration of particles and bubbles settling or rising near vertical walls at moderate *Re*. Empirical estimates of the transverse force, like (6) for contaminated bubbles and rigid spheres or (8) for clean bubbles, may be used in practical calculations to obtain a crude evaluation of the effect of this force on the overall flow, especially to determine the radial distribution of bubbles and particles in pipes. Nevertheless, it must be kept in mind that these expressions have limitations, especially for small separations. Full numerical simulations, possibly including effects of deformation, are highly desirable in order to obtain more accurate and more complete variations of the lift force and of the transverse history force over the full range of particle Reynolds number and separation from the wall.

We are indebted to Dr D. Legendre and Dr S. Takagi for helpful discussions on the problem addressed in this work.

REFERENCES

Batchelor, G. K. 1967 *An Introduction to Fluid Dynamics*. Cambridge University Press.

Biesheuvel, A. & van Wijngaarden, L. 1982 The motion of pair of gas bubbles in a perfect liquid. *J. Engng Maths* **16**, 349–365.

Clift, R., Grace, J. R. & Weber, M. E. 1978 *Bubbles, Drops and Particles*. Academic.

Cox, R. G. & Hsu, S. K. 1977 The lateral migration of solid particles in a laminar flow near a plate. *Intl J. Multiphase Flow* **3**, 201–222.

Duineveld, P. C. 1995 The rise velocity and shape of bubbles in pure water at high Reynolds number. *J. Fluid Mech.* **292**, 325–332.

KIM, I., ELGOBASHI, S. & SIRIGNANO, W. A. 1993 Three-dimensional flow over two spheres placed side by side. *J. Fluid Mech.* **246**, 465–488.

KOK, J. B. W. 1993 Dynamics of a pair of gas bubbles moving through liquid. Part I. Theory. *Eur. J. Mech.* B/*Fluids* **12**, 515–540.

LEGENDRE, D. & MAGNAUDET, J. 1997 A note on the lift force on a spherical bubble or drop in a low-Reynolds-number shear flow. *Phys. Fluids* **9**, 3572–3574.

LOVALENTI, P. M. & BRADY, J. F. 1993 The force on a bubble, drop, or particle in arbitrary time-dependent motion at small Reynolds number. *Phys. Fluids* A **5**, 2104–2116.

MAGNAUDET, J. & EAMES, I. 2000 The motion of high-Reynolds-number bubbles in inhomogeneous flows. *Annu. Rev. Fluid Mech.* **32**, 659–708.

MAGNAUDET, J., RIVERO, M. & FABRE, J. 1995 Accelerated flows past a rigid sphere or a spherical bubble. Part I. Pure straining flow. *J. Fluid Mech.* **284**, 97–135.

MAGNAUDET, J., TAKAGI, S. & LEGENDRE, D. 2003 Drag, deformation and lateral migration of a buoyant drop moving near a wall. *J. Fluid Mech.* **476**, 115–157.

MEI, R. & KLAUSNER, J. F. 1992 Unsteady force on a spherical bubble at finite Reynolds number with small fluctuations in the free-stream velocity. *Phys. Fluids* A **4**, 63–70.

MEI, R., KLAUSNER, J. F. & LAWRENCE, C. J. 1994 A note on the history force on a spherical bubble at finite Reynolds number. *Phys. Fluids* **6**, 418–420.

MILNE-THOMSON, L. M. 1968 *Theoretical Hydrodynamics.* Macmillan.

MILOH, T. 1977 Hydrodynamics of deformable contiguous spherical shapes in an incompressible inviscid fluid. *J. Engng Maths* **11**, 349–372.

MOORE, D. W. 1963 The boundary layer on a spherical gas bubble. *J. Fluid Mech.* **16**, 161–176.

TAKEMURA, F., TAKAGI, S., MAGNAUDET, J. & MATSUMOTO, Y. 2002 Drag and lift forces on a bubble rising near a vertical wall in a viscous liquid. *J. Fluid Mech.* **461**, 277–300.

TAKEMURA, F. & YABE, A. 1999 Rising speed and dissolution rate of a carbon dioxide bubble in slightly contaminated water. *J. Fluid Mech.* **378**, 319–334.

TSAO, H. K. & KOCH, D. L. 1994 Collision of slightly deformable, high Reynolds number bubbles with short-range repulsive forces. *Phys. Fluids* **6**, 2591–2605.

VASSEUR, P. & COX, R. G. 1977 The lateral migration of spherical particles sedimenting in a stagnant bounded fluid. *J. Fluid Mech.* **80**, 561–591.

DE VRIES, A. W. G. 2001 Path and wake of a rising bubble. PhD thesis, Twente University, The Netherlands.

YANG, S. & LEAL, L. G. 1991 A note on memory-integral contributions to the force on an accelerating spherical drop at low Reynolds number. *Phys. Fluids* A **3**, 1822–1823.